

Published in final edited form as:

Phys Med Biol. 2008 January 7; 53(1): 279–293.

In vivo visualization of abdominal malignancies with acoustic radiation force elastography

B J Fahey¹, R C Nelson², D P Bradway¹, S J Hsu¹, D M Dumont¹, and G E Trahey^{1,2}

¹*Department of Biomedical Engineering, Duke University, Durham, NC, USA*

²*Department of Radiology, Duke University, Durham, NC, USA*

Abstract

The utility of acoustic radiation force impulse (ARFI) imaging for real-time visualization of abdominal malignancies was investigated. Nine patients presenting with suspicious masses in the liver ($n = 7$) or kidney ($n = 2$) underwent combined sonography/ARFI imaging. Images were acquired of a total of 12 tumors in the nine patients. In all cases, boundary definition in ARFI images was improved or equivalent to boundary definition in B-mode images. Displacement contrast in ARFI images was superior to echo contrast in B-mode images for each tumor. The mean contrast for suspected hepatocellular carcinomas (HCCs) in B-mode images was 2.9 dB (range: 1.5–4.2) versus 7.5 dB (range: 3.1–11.9) in ARFI images, with all HCCs appearing more compliant than regional cirrhotic liver parenchyma. The mean contrast for metastases in B-mode images was 3.1 dB (range: 1.2–5.2) versus 9.3 dB (range: 5.7–13.9) in ARFI images, with all masses appearing less compliant than regional non-cirrhotic liver parenchyma. ARFI image contrast (10.4 dB) was superior to B-mode contrast (0.9 dB) for a renal mass. To our knowledge, we present the first *in vivo* images of abdominal malignancies in humans acquired with the ARFI method or any other technique of imaging tissue elasticity.

1. Introduction

Effective visualization of potentially malignant masses is of paramount importance during both the diagnostic and treatment stages of patient care. This is particularly true during interventional procedures, where the significance of accurate, convenient and cost-efficient imaging mechanisms for guiding device placement has become increasingly evident. Accurate placement of interventional devices is vital to the success of both targeted biopsies (Charboneau *et al* 1990) and minimally invasive ablative therapies (De Baere *et al* 2000, Antoch *et al* 2002, Veit *et al* 2006). Depending on the personal preferences of the intervening radiologist and the location and tissue properties of the target mass, procedure guidance is generally performed using ultrasound (US) (Sheafor *et al* 1998, Rose *et al* 2001, Won *et al* 2003, Paulsen *et al* 2006), CT (Wood *et al* 1999, Mayo-Smith *et al* 2003) or MR (Konig *et al* 2004, Silverman *et al* 2004, Kariniemi *et al* 2005) methods. Each of these imaging modalities is associated with inherent advantages and limitations.

When feasible, sonography is the guidance method of choice at many institutions for procedures targeting the liver, kidneys, pancreas and lymph nodes (Paulsen *et al* 2006, Sheafor *et al* 1998, Won *et al* 2003, Johnson *et al* 2001, Tang *et al* 2002). Advantages of US include widespread availability, real-time operation, relatively low cost and the lack of ionizing radiation. The use of US as a guidance mechanism also generally reduces the procedure time relative to cases where other guidance modalities are used (Sheafor *et al* 1998, 2000). However, a significant portion of patients present with masses that are difficult to visualize by US. These masses may be isoechoic, deeply located (Charboneau *et al* 1990) or positioned in difficult regions such as the hepatic dome (Lu *et al* 1997). In these patients CT without or with CT fluoroscopy may be useful to guide the placement of an interventional device (Antoch *et al*

2002, Paulsen *et al* 2006, Mayo-Smith *et al* 2003), although real-time placement is rarely implemented, given the radiation exposures involved (particularly to the operator) (Sheafor *et al* 2000, Daly *et al* 1999). The iterative nature of this method significantly increases the cost and time requirements of the procedure. Additionally, given the case of isodense and/or non-enhancing lesions, CT visualization may not be adequate for accurate device placement (Veit *et al* 2006). For these cases, methods such as MR or combined PET/CT have been investigated (Veit *et al* 2006, Konig *et al* 2004, Silverman *et al* 2004, Kariniemi *et al* 2005, Lu *et al* 1997, Kelekis *et al* 2003). Although these guidance methods may allow for accurate device placement in masses not well visualized with US or CT, the incorporation of these modalities markedly increases the complexity and cost of the procedure (Veit *et al* 2006, Kariniemi *et al* 2005).

New and/or hybrid imaging modalities may offer key advantages for visualization and interventional guidance for difficult masses. For example, a number of research institutions are currently investigating the utility of various methods of imaging soft tissue elasticity. These methods (summarized in a review by Greenleaf *et al* (2003)) interrogate tissue mechanical properties and produce images that are generally representative of underlying tissue stiffness. Elasticity imaging methods have shown clinical promise for *in vivo* detection of malignancies located in the breast (Cespedes *et al* 1993, Garra *et al* 1997, McKnight *et al* 2002, Bercoff *et al* 2003, Sharma *et al* 2004, Sinkus *et al* 2005, Itoh *et al* 2006, Insana *et al* 2004), prostate (Lorenz *et al* 1999, Cochlin *et al* 2002, Souchon *et al* 2003, Sommerfeld *et al* 2003, Konig *et al* 2005) and other organs (Chakraborty *et al* 2006, Lyshchik *et al* 2005). Further, direct mechanical measurements of resected liver samples have indicated that elastic contrast also exists for many tumors in the liver (Yeh *et al* 2002). Despite this finding, research evaluating the effectiveness of elasticity imaging methods to visualize human abdominal masses *in vivo* has been very limited (Emelianov *et al* 1998) (although diffuse liver and kidney diseases have been examined by many groups (Sanada *et al* 2000, Sandrin *et al* 2003, Weitzel *et al* 2004, Foucher *et al* 2006, Huwart *et al* 2006, Klatt *et al* 2006, Rouviere *et al* 2006)). Establishing the feasibility of adequate abdominal tumor visualization with elasticity imaging is a fundamental step toward demonstrating the potential of utilizing these techniques to guide the placement of interventional devices.

Previous efforts have demonstrated the utility of acoustic radiation force impulse (ARFI) imaging for abdominal applications and noted some advantages of the ARFI technique for imaging at depth (Fahey *et al* 2005, 2006b). In the current study, we investigate the feasibility of visualizing abdominal malignancies using the ARFI method. We provide images of liver and kidney tumors that are, to the best of our knowledge, the first *in vivo* elasticity images presented of malignant masses in these organs in humans. CT images of target regions are provided for comparative purposes. ARFI imaging is an ultrasound-based modality implemented entirely on a modified diagnostic scanner and is designed for complementary use with conventional real-time sonography. Thus, the use of a combined sonography/ARFI imaging system to aid in the placement of interventional devices would provide a clinician with information about tissue mechanical properties while retaining all of the benefits of US guidance.

2. Materials and methods

2.1. Patient population and imaging protocol

To date, nine consecutive patients have been recruited in an ongoing study approved by and conducted in full accordance with the guidelines established by the Duke University Medical Center (DUMC) Institutional Review Board. The subject population included five men and four women with a mean age of 60 years (range: 46-83 years). Patients eligible for inclusion had been admitted to DUMC and were scheduled for biopsy ($n = 3$) or treatment ($n = 6$) of

suspicious masses in the liver ($n = 7$) and/or kidney ($n = 2$). Prior knowledge concerning the size, location or ultrasonic appearance of target masses was not utilized to determine patient eligibility and did not impact patient recruitment. One patient re-enrolled in the study when he returned for a second treatment (for a newly developed tumor) approximately 7 months following his initial participation. A second patient presented with masses in both the liver and kidney that were later determined to originate from primary renal cell cancer. Interventional treatments and experimental images in this patient were focused upon the liver masses, and thus this patient has been classified into the 'liver' patient subset. Data were acquired of a total of 12 tumors in the nine unique patients included in the study. Target masses were located at depths ranging from 2 to 10 cm. Written consent was obtained from all patients prior to their inclusion in the study.

All patient data were collected immediately prior to the scheduled interventional procedure. Experimental data were acquired using a Siemens SONOLINE Antares™ scanner (Siemens Medical Solutions USA, Inc., Ultrasound Division, Issaquah, WA) that has been modified to allow for custom beam sequencing and access to raw radiofrequency (RF) data. A Siemens CH4-1 curvilinear transducer array operating at 2.2 or 1.8 MHz was used during data acquisition. In each patient, B-mode ultrasound and ARFI images were acquired in regions of interest. B-mode images were acquired both as a standard screen capture using Siemens processing algorithms and as a reconstructed image created from raw RF data using custom processing algorithms. Although screen capture images were generally qualitatively superior, only the reconstructed images allowed for the calculation of contrast and precise anatomic registration with ARFI images. Screen capture images were acquired beginning with the 4th overall patient included in the study. All image data were collected during a patient breath hold. When possible without interfering with patient access, ECG gating was also utilized during data acquisition to minimize cardiovascular-related tissue motion in regions of interest (Fahey *et al* 2007). A 3 pixel \times 3 pixel spatial median filter was applied to all ARFI images prior to display.

B-mode and ARFI images were compared both qualitatively and quantitatively. Qualitative analyses included assessments of lesion boundary definition by observers both blinded to and familiar with gold-standard MR or CT data acquired as part of the patients' standard of care. Quantitative analyses included the calculation of image contrast. Echo contrast was calculated using envelope-detected RF (i.e., B-mode image) data saved during experimental imaging. Values stated in the text were calculated after log compression of B-mode image pixel magnitude, since virtually all diagnostic scanners log compress B-mode image data prior to display. However, for perspective, contrast values calculated from linearly scaled B-mode image data are provided in the complete data table. Displacement contrast was calculated from raw ARFI image displacement data.

Contrast calculations were performed using rectangular regions of interest (ROIs) that were selected both inside target lesions and in adjacent non-tumorous tissues. ROI location was chosen by the consensus of two observers after examination of B-mode and ARFI image data. ROIs within lesions were chosen to be as large as possible while confidently remaining within tumor boundaries. ROIs in adjacent non-tumorous tissues were assigned to be of the same size and shape as the corresponding region within the tumor. For each data set, the ROIs used for B-mode and ARFI image contrast calculations were identical. Contrast was calculated using the following formula:

$$\text{Contrast} = |20 \times \log\left(\frac{M_b}{M_l}\right)|, \quad (1)$$

where M_b and M_l are the mean B-mode or ARFI pixel magnitudes inside the non-tumorous background tissue and lesion ROIs, respectively.

Imaging planes were selected in an attempt to center target lesions (those being biopsied or treated) in the ARFI image field-of-view (FOV). Analyses focused upon these target tumors. In some cases, additional tumors were contained in the image FOV. Uncertainties regarding the total size of these lesions and the percentage of lesion volume contained within the imaging plane led to the exclusion of these tumors from analysis.

CT or MR images acquired as part of the patients' standard of care were collected for reference. In all instances, indications present on MR and/or CT motivated referral to interventional clinics, and thus these reference images were acquired in the week(s) (range: 1-9 weeks) leading up to experimental ARFI imaging sessions. When possible, the ARFI imaging plane was chosen to be similar to cross-sections available with these other modalities, although limited acoustic windows and other factors (such as the oblique planes used commonly during free-hand US imaging) prohibited precise correspondence in many patients. Due to difficulties associated with consistent plane registration of experimental and reference imaging modalities, a comprehensive comparison of lesion size in ARFI images to gold-standard reference measurements is not performed in this study. For a thorough analysis of the accuracy of cross-sectional area and volume measurements made with ARFI imaging, the reader is referred to previous studies (Fahey *et al* 2006a).

2.2. Acoustic radiation force and ARFI imaging

Acoustic radiation force is a phenomenon associated with the propagation of acoustic waves through a dissipative medium. The force originates from a transfer of momentum from the wave to the medium, arising either from absorption or reflection of the wave (Torr 1984). In absorbing media (such as soft tissue), this body force (and the resulting tissue displacement) is in the direction of wave propagation.

ARFI imaging uses short duration (0.03-0.4 ms) pulses of ultrasound to excite target tissues. The dynamic response of tissues to impulsive radiation forces is recorded in the region of excitation using standard diagnostic ultrasound pulses transmitted at pulse repetition frequencies (PRFs) ranging from 3 to 12 kHz. Although 2D tissue tracking algorithms have been implemented, in most applications the tissue response is monitored solely in the direction of beam propagation. The tissue displacement/recovery behavior is calculated using ultrasonic correlation-based or Doppler methods (Kasai *et al* 1985, Trahey *et al* 1987, O'Donnell *et al* 1994).

The tissue response to radiation force is monitored spatially as well as temporally. Two-dimensional ARFI images are made by electronically translating the active transducer aperture to interrogate a new region of tissue. Acquisition times are a function of the line density, FOV and the temporal period over which each tissue region is monitored, and do not exceed 350 ms in most applications.

Assuming a uniform distribution of radiation force, the magnitude of induced tissue displacement is generally inversely related to tissue stiffness. The tissue recovery response is related to tissue's viscoelastic properties (Nightingale *et al* 2003), most notably its shear modulus. In the focal region, the peak magnitude of resulting tissue displacement is typically on the order of 5-20 μm , with tissue recovery times ranging from 1 to 10 ms.

Previous investigations have examined the potential of ARFI imaging to induce potentially harmful mechanical or thermal bioeffects (Palmeri and Nightingale 2004, Nightingale *et al* 2002). The radiation force beams used during ARFI imaging are similar to those used during color Doppler imaging. For abdominal applications, typical spatial-peak, pulse-average intensities (I_{SPPA}) are on the order of 820 W cm^{-2} in the focal region. Radiation force beams

generally have pulse lengths on the order of 100-300 μ s. For abdominal applications, these pulses have a beam width on the order of 2 mm in the focal zone.

ARFI imaging is implemented entirely on a modified diagnostic US scanner. Other than a laptop computer used to control data acquisition, no additional equipment is required for ARFI imaging. A single transducer is used to apply radiation force to tissues and to monitor the ensuing tissue dynamics. The use of an US platform allows for co-registered B-mode, color Doppler and ARFI images to be generated while retaining the portability and low operating costs associated with sonography.

3. Results

3.1. Quantitative analysis

Table 1 provides a list of the image contrast values associated with the tumors encountered in this study. Several of the tumors in the table are provided as example images in this manuscript and are labeled accordingly. All tumors not shown as example images (labeled as 'NS' in the table) were metastases in non-cirrhotic liver. As indicated, displacement contrast in ARFI images is superior to echo contrast in (both log-compressed and linearly scaled) B-mode images for every mass imaged to date. The mean contrast for suspected hepatocellular carcinomas (HCCs) in B-mode images was 2.9 dB (range 1.5-4.2) versus 7.5 dB (range 3.1-11.9) in ARFI images, with all HCCs appearing more compliant (i.e., brighter) than regional cirrhotic non-tumorous liver parenchyma. The mean contrast for hepatic metastases in B-mode images was 3.1 dB (range 1.2-5.2) versus 9.3 dB (range 5.7-13.9) in ARFI images, with all appearing relatively less compliant (i.e., darker) than regional non-cirrhotic, non-tumorous liver parenchyma.

There was one mass in the study (a renal malignancy being treated with cryoablation therapy) that was visualized poorly with both US and ARFI methods. Since the location of the mass in the resulting images was ambiguous, accurate contrast measurements could not be made. Data for this mass are therefore not included in table 1. Factors leading to poor visualization included patient obesity, phase aberration effects and deep (12+ cm) scan depths.

3.2. Imaging examples

Figures 1 and 2 show images from a 62-year-old male who was scheduled for biopsy after multiple suspicious liver masses were found with CT. Sonographic examination revealed the presence of several hypoechoic masses located throughout the liver. Biopsy results confirmed the presence of metastatic disease, likely originating from primary pancreatic cancer.

Figures 1(a) and (b) show transverse reconstructed B-mode and ARFI images, respectively, of a 2 cm metastasis in the left hepatic lobe. The mass appears slightly hypoechoic in the B-mode image and in the ARFI image as a dark region of low ($<5 \mu$ m) displacement that is surrounded by more compliant (displacements larger than 12μ m) non-tumorous liver parenchyma (see arrows). Contrast of the mass is 4.6 dB in (a) and 13.9 dB in (b).

Figures 2(a) and (b) show longitudinal reconstructed B-mode and ARFI images in a different region in the same patient. Contained in the imaging plane are two metastases (the target mass is denoted in (b) by the broken arrow, a second mass found incidentally is denoted by the black arrow) and a portion of the heart (solid white arrow). Both masses appear hypoechoic in the B-mode image and as dark regions of relatively stiff tissue (reduced displacement magnitude) in the ARFI image. Displacement contrast of the target mass in the ARFI image (9.7 dB) is greater than echo contrast in the reconstructed B-mode image (2.6 dB).

Figure 3 shows images from a 66-year-old male patient acquired immediately prior to RF ablation treatment of a 3.5×3.6 cm suspicious mass in the right hepatic lobe. The patient was known to have hepatitis C, cirrhosis and to be HIV-positive. Given the setting of cirrhosis and elevated α -fetoprotein (AFP) levels, this newly developed mass was clinically diagnosed as a HCC and treated accordingly (Nguyen *et al* 2003).

Figures 3(a) and (b) show screen capture B-mode and ARFI images, respectively, of the HCC. The target malignancy is seen in (a) as a slightly hyperechoic structure surrounded by a hypoechoic fibrous capsule. In (b), the malignancy is shown as a bright region (arrow) of relatively high displacement ($6-8 \mu\text{m}$) that is surrounded by the stiff fibrous capsule (arrow heads). The remaining, non-tumorous liver tissue appears with relatively uniform but small ($5 \mu\text{m}$) displacement, consistent with bulk stiffening due to cirrhosis (Yeh *et al* 2002, Sandrin *et al* 2003, Ziol *et al* 2005). Again, ARFI image contrast (11.9 dB) exceeds B-mode image contrast (4.2 dB).

Figure 4 shows images of a 47-year-old female patient scheduled for a targeted liver biopsy. Previous examinations had confirmed the presence of liver cirrhosis and indicated several small (1-2 cm) lesions in the left lobe, fairly close to the anterior abdominal wall. Figures 4(a) and (b) show transverse reconstructed B-mode and ARFI images, respectively, acquired of the lesion prior to biopsy. In (a), the target mass is visualized as a low contrast hypoechoic structure (arrows) centered in the FOV. In (b), the mass is shown to be relatively compliant (bright) and surrounded by stiff non-tumorous liver parenchyma (consistent with the HCC shown in figure 3). Displacement magnitude in cirrhotic liver tissue (in this case, $6-8 \mu\text{m}$) is reduced relative to displacement magnitudes induced with identical ARFI beam sequences in non-cirrhotic patients (for example, see figures 1 and 2).

Figure 5 shows images of a 54-year-old male patient prior to cryoablative treatment of an 18 mm mass in the lower pole of the left kidney. The newly developed solid renal mass was diagnosed as renal cell carcinoma (RCC) based upon findings available through CT imaging (Miller 1999). Transverse B-mode and ARFI images are shown in (a) and (b), respectively. Although the kidney is well visualized in (a) (see arrows), the renal malignancy is nearly imperceptible. The malignancy is better visualized in (b) as a dark region of low displacement at the edge of the kidney (indicated by solid arrows). Contrast of the tumor is 10.4 dB in the ARFI image and 0.9 dB in the B-mode image.

4. Discussion

The results presented in the previous section establish the feasibility of visualizing liver and kidney malignancies with ARFI imaging. We believe that these are the first human images of abdominal malignancies acquired *in vivo* using the ARFI method or any other elasticity of imaging technique. Our preliminary data suggest that the ARFI method can provide improvements in boundary definition and contrast of tissue masses relative to the use of sonography alone. For all of the cases encountered to date, displacement contrast of both primary and secondary malignancies in ARFI images has been larger than echo contrast in conventional B-mode US images.

In general, boundary definition of lesions in ARFI images was superior to that seen in both screen capture and reconstructed B-mode images. In particular, the anterior margins of some tumors (located in the near field of the imaging system) were difficult to characterize in B-mode images. Improved visualization of tumor margins was achieved with ARFI imaging, although in several cases some tumor boundaries remained ambiguous. Intra-observer agreement between readers assessing pairs of B-mode and ARFI images was generally very good. Given the nature of this feasibility study and the limited number of lesions analyzed to

date, a formal statistical analysis related to potential improvements in boundary definition has yet to be performed.

ARFI imaging can easily and inexpensively be integrated into imaging protocols already involving the use of conventional US, and thus a combined sonography/ARFI system may be a viable and useful platform for detecting and characterizing focal lesions and for guiding the placement of interventional devices. Sonography is the preferred method at many institutions for guiding device insertion, but its application remains limited by poor visualization of some target masses. Several of the cases encountered to date (for example, see figure 5) involved isoechoic target malignancies. These cases required extensive patient exposure to ionizing radiation from CT and CT-based fluoroscopic imaging for accurate device placement during treatment. Although it would be premature to suggest that a combined sonography/ARFI system could replace CT or MR methods for insertion guidance, the use of such a system could potentially reduce the reliance on these more expensive and complicated modalities. Although further investigation is required, it is likely that ARFI imaging could provide additional pertinent information to an interventionalist without increasing the cost or time requirements of a procedure.

Combined sonography/ARFI may also find use for tumor screening, lesion characterization and early detection of disease. HCC is the fifth most common cancer (Okuda 2000), and curative treatment options available for early stage HCC are generally not available once the tumor reaches the intermediate or advanced stages (Livraghi *et al* 2004). Despite this, screening for HCC is not considered cost-effective in regions with low prevalence, partially due to the low sensitivity of both sonography and AFP testing for this purpose (Yuen and Lai 2003). Given a low cost, real-time imaging system capable of improving tumor contrast relative to using sonography alone, improvements in sensitivity and cost-efficiency may be achievable. The compliant mechanical nature of HCCs may also serve as a distinguishing feature, leading to an increase in specificity. Currently, the sensitivity and specificity of combined sonography/ARFI imaging for this purpose is unknown. Future large-scale studies are required to determine these metrics and to evaluate the screening improvements that have been hypothesized.

Outside of the United States, contrast-enhanced ultrasound (CEUS) has been established as a viable method for lesion detection and characterization and for assistance with interventional procedures in the liver (Burns *et al* 2000, Choi *et al* 2002, Solbiati *et al* 1999). To our knowledge, studies comparing the effectiveness of CEUS to any implementation of elasticity imaging are not reported in the literature. If ARFI imaging is proven to be a feasible alternative to CEUS for liver applications, it may hold potential advantages related to the cost and complexity of the imaging protocol.

The onset of fibrosis and cirrhosis in the liver is known to correspond with changes in the bulk elasticity of the organ. Accordingly, elasticity imaging methods have shown significant promise for assessment of diffuse liver disease (Sanada *et al* 2000, Sandrin *et al* 2003, Foucher *et al* 2006, Huwart *et al* 2006, Klatt *et al* 2006, Rouviere *et al* 2006). Preliminary quantitative *in vivo* results indicate that the ARFI method may also find use for this application (Nightingale *et al* 2006). Although the present study has not attempted to reconstruct a tissue elastic modulus, the results presented herein indicate significantly lower displacement magnitudes induced in cirrhotic liver tissues relative to those induced in non-cirrhotic liver tissues. The ability to measure bulk liver stiffness while simultaneously screening for focal lesions is one advantage of ARFI imaging that is not associated with many other ultrasound-based methods of imaging tissue elasticity.

Tumors encountered in this study had diameters ranging from 1 to 4.5 cm and were located at depths ranging from 2 to 10 cm. From the initial results, no correlation was observed between

ARFI image contrast or quality and either the depth or size of target lesions. However, acoustic attenuation effects currently limit achievable displacement magnitude in regions deeper than 10-12 cm. For deeper lying lesions, the use of lower transmit frequencies for radiation force pulses will likely prove advantageous.

The current study has several limitations, the most significant of which is likely the small number of patients included to date. Although we have been able to reach preliminary conclusions based upon our initial experiences, a more extensive study is required to confirm these findings and to establish the consistency of the ARFI method. It is also probable that some patients will present with masses having properties that differ from those encountered thus far. For instance, it is likely that in some masses echo contrast will exceed displacement contrast. Additionally, the mechanical response of benign abdominal masses to applied radiation forces has yet to be determined, and thus the ability of ARFI imaging to differentiate benign from malignant masses is largely unknown. Further, a formal study of the intra- and inter-operator reproducibility of the ARFI technique has yet to be performed. Future efforts will expand upon these initial results in order to more completely assess the utility of abdominal ARFI imaging.

A second limitation to our study is that thus far we have only acquired experimental images before and after (not during) the placement of interventional devices. Our initial focus was to establish the feasibility of consistent high-quality visualization of abdominal malignancies. Although we have hypothesized that the use of a combined sonography/ARFI system will aid in the placement of interventional devices, we have yet to collect any evidence to support this claim. A dedicated study comparing both the accuracy and the time and cost requirements of different image guidance mechanisms for device placement into masses with low echo contrast is necessary to evaluate this possibility.

In summary, we have presented the initial results from our clinical investigations into the utility of ARFI imaging for abdominal applications. Data collected to date indicate that ARFI imaging improves visualization of malignancies in the liver and kidney compared to the use of conventional US alone. In cirrhotic liver, suspected hepatocellular carcinomas were shown to be more compliant than regional liver. In non-cirrhotic liver, metastases were shown to be less compliant than regional liver. As ARFI imaging is ultrasound based, combined sonography/ARFI scanning is a straightforward and inexpensive technique that allows for the strengths of the two modalities to be utilized in a highly complementary manner. Given the promising results encountered thus far, we believe that ARFI imaging has potential to become a valuable clinical tool.

Acknowledgments

The authors would like to thank the nurses and staff at DUMC for their assistance with coordinating our clinical efforts. In particular, the studies would not have been possible without the aid of Mitzi Chambers or Susan Hunter. The authors thank Siemens Medical Solutions, USA, Ultrasound Division, for their system support. This work was supported by NIH Grants 1R01-HL-075485-02, 1R01-EB-002132-04 and 1R01-CA-114093-01.

References

- Antoch G, Kuehl H, Vogt FM, Debatin JF, Stattaus J. Value of CT volume imaging for optimal placement of radiofrequency ablation probes in liver lesions. *J. Vasc. Interv. Radiol* 2002;13:1155–61. [PubMed: 12427816]
- Bercoff J, Chaffai S, Tanter M, Sandrin L, Catheline S, Fink M, Gennisson JL, Meunier M. *In vivo* breast tumor detection using transient elastography. *Ultrasound Med. Biol* 2003;29:1387–96. [PubMed: 14597335]

- Burns PN, Wilson SR, Simpson DH. Pulse inversion imaging of liver blood flow: improved method for characterizing focal masses with microbubble contrast. *Invest. Radiol* 2000;35:58–71. [PubMed: 10639037]
- Cespedes I, Ophir J, Ponnekanti H, Maklad N. Elastography: elasticity imaging using ultrasound with application to muscle and breast *in vivo*. *Ultrason. Imaging* 1993;15:73–88. [PubMed: 8346612]
- Chakraborty A, Berry G, Bamber J, Dorward N. Intra-operative ultrasound elastography and registered magnetic resonance imaging of brain tumours: a feasibility study. *Ultrasound* 2006;14:43–9.
- Charboneau JW, Reading CC, Welch TJ. CT and sonographically guided needle biopsy: current techniques and new innovations. *AJR Am. J. Roentgenol* 1990;154:1–10. [PubMed: 2104689]
- Choi D, Lim HK, Kim SH, Lee WJ, Jang HJ, Kim H, Lee SJ, Lim JH. Assessment of therapeutic response in hepatocellular carcinoma treated with percutaneous radio frequency ablation: comparison of multiphase helical computed tomography and power Doppler ultrasonography with a microbubble contrast agent. *J. Ultrasound Med* 2002;21:391–401. [PubMed: 11934096]
- Cochlin DL, Ganatra RH, Griffiths DF. Elastography in the detection of prostatic cancer. *Clin. Radiol* 2002;57:1014–20. [PubMed: 12409113]
- Daly B, Krebs TL, Wong-You-Cheong JJ, Wang SS. Percutaneous abdominal and pelvic interventional procedures using CT fluoroscopy guidance. *AJR Am. J. Roentgenol* 1999;173:637–44. [PubMed: 10470894]
- De Baere T, et al. Radiofrequency ablation of 100 hepatic metastases with a mean follow-up of more than 1 year. *AJR Am. J. Roentgenol* 2000;175:1619–25. [PubMed: 11090390]
- Emelianov S, Rubin J, Lubinski M, Skovoroda A, O'donnell M. Elasticity imaging of the liver: is a hemangioma hard or soft? Proc. 1998 IEEE Ultrasonics Symposium (IEEE). 1998
- Fahey BJ, Dumont DM, Trahey GE. Volume visualization and error analysis using 3D ARFI imaging data. Proc. 2006 IEEE Ultrasonics Symposium (IEEE). 2006a
- Fahey BJ, Hsu SJ, Wolf PD, Nelson RC, Trahey GE. Liver ablation guidance with acoustic radiation force impulse imaging: challenges and opportunities. *Phys. Med. Biol* 2006b;51:3785–808. [PubMed: 16861781]
- Fahey BJ, Nightingale KR, Nelson RC, Palmeri ML, Trahey GE. Acoustic radiation force impulse imaging of the abdomen: demonstration of feasibility and utility. *Ultrasound Med. Biol* 2005;31:1185–98. [PubMed: 16176786]
- Fahey BJ, Palmeri ML, Trahey GE. The impact of physiological motion on tissue tracking during radiation force imaging. *Ultrasound Med. Biol* 2007;33:1149–66. [PubMed: 17451869]
- Foucher J, Castera L, Bernard PH, Adhoute X, Laharie D, Bertet J, Couzigou P, De Ledinghen V. Prevalence and factors associated with failure of liver stiffness measurement using FibroScan in a prospective study of 2114 examinations. *Eur. J. Gastroenterol. Hepatol* 2006;18:411–2. [PubMed: 16538113]
- Garra BS, Cespedes EI, Ophir J, Spratt SR, Zuurbier RA, Magnant CM, Pennanen MF. Elastography of breast lesions: initial clinical results. *Radiology* 1997;202:79–86. [PubMed: 8988195]
- Greenleaf JF, Fatemi M, Insana M. Selected methods for imaging elastic properties of biological tissues. *Annu. Rev. Biomed. Eng* 2003;5:57–78. [PubMed: 12704084]
- Huwart L, Peeters F, Sinkus R, Annet L, Salameh N, Ter Beek LC, Horsmans Y, Van Beers BE. Liver fibrosis: non-invasive assessment with MR elastography. *NMR Biomed* 2006;19:173–9. [PubMed: 16521091]
- Insana MF, Pellot-Barakat C, Sridhar M, Lindfors KK. Viscoelastic imaging of breast tumor microenvironment with ultrasound. *J. Mammary Gland Biol. Neoplasia* 2004;9:393–404. [PubMed: 15838608]
- Itoh A, Ueno E, Tohno E, Kamma H, Takahashi H, Shiina T, Yamakawa M, Matsumura T. Breast disease: clinical application of US elastography for diagnosis. *Radiology* 2006;239:341–50. [PubMed: 16484352]
- Johnson PT, Nazarian LN, Feld RI, Needleman L, Lev-Toaff a S, Segal SR, Halpern EJ. Sonographically guided renal mass biopsy: indications and efficacy. *J. Ultrasound Med* 2001;20:749–53. [PubMed: 11444733]quiz 55
- Kariniemi J, Blanco Sequeiros R, Ojala R, Tervonen O. MRI-guided abdominal biopsy in a 0.23-T open-configuration MRI system. *Eur. Radiol* 2005;15:1256–62. [PubMed: 15627187]

- Kasai C, Namekawa K, Koyano A, Omoto R. Real-time two-dimensional blood flow imaging using an auto-correlation technique. *IEEE Trans. Son. Ultrason* 1985;32:458–64.
- Kelekis AD, Terraz S, Roggan A, Terrier F, Majno P, Mentha G, Roth A, Becker CD. Percutaneous treatment of liver tumors with an adapted probe for cooled-tip, impedance-controlled radio-frequency ablation under open-magnet MR guidance: initial results. *Eur. Radiol* 2003;13:1100–5. [PubMed: 12695834]
- Klatt D, Asbach P, Rump J, Papazoglou S, Somasundaram R, Modrow J, Braun J, Sack I. *In vivo* determination of hepatic stiffness using steady-state free precession magnetic resonance elastography. *Invest. Radiol* 2006;41:841–8. [PubMed: 17099421]
- Konig K, Scheipers U, Pesavento A, Lorenz A, Ermert H, Senge T. Initial experiences with real-time elastography guided biopsies of the prostate. *J. Urol* 2005;174:115–7. [PubMed: 15947593]
- Konig CW, Trubenbach J, Fritz J, Lauer UM, Claussen CD, Pereira PL. Contrast enhanced MR-guided biopsy of hepatocellular carcinoma. *Abdom. Imaging* 2004;29:71–6. [PubMed: 15160756]
- Livraghi T, Meloni F, Morabito A, Vettori C. Multimodal image-guided tailored therapy of early and intermediate hepatocellular carcinoma: long-term survival in the experience of a single radiologic referral center. *Liver Transplant* 2004;10:S98–106.
- Lorenz A, Sommerfeld H, Garcia-Schurmann M, Philippou S, Senge T, Ermert H. A new system for the acquisition of ultrasonic multicompression strain images of the human prostate *in vivo*. *IEEE Trans. Ultrason. Ferroelectr. Freq. Control* 1999;46:1147–54. [PubMed: 18244308]
- Lu DS, Lee H, Farahani K, Sinha S, Lufkin R. Biopsy of hepatic dome lesions: semi-real-time coronal MR guidance technique. *AJR Am. J. Roentgenol* 1997;168:737–9. [PubMed: 9057526]
- Lyshchik A, et al. Thyroid gland tumor diagnosis at US elastography. *Radiology* 2005;237:202–11. [PubMed: 16118150]
- Mayo-Smith WW, Dupuy DE, Parikh PM, Pezzullo JA, Cronan JJ. Imaging-guided percutaneous radiofrequency ablation of solid renal masses: techniques and outcomes of 38 treatment sessions in 32 consecutive patients. *AJR Am. J. Roentgenol* 2003;180:1503–8. [PubMed: 12760909]
- Mcknight AL, Kugel JL, Rossman PJ, Manduca A, Hartmann LC, Ehman RL. MR elastography of breast cancer: preliminary results. *AJR Am. J. Roentgenol* 2002;178:1411–7. [PubMed: 12034608]
- Miller K. Renal cell carcinoma: guidelines for diagnosis and treatment. *Urologia Internationalis* 1999;63:6–9. [PubMed: 10592483]
- Nguyen M, Garcia R, Simpson P, Wright T, Keefe E. Racial differences in effectiveness of alpha-fetoprotein for diagnosis of hepatocellular carcinoma in hepatitis C virus cirrhosis. *Hepatology* 2003;36:410–7. [PubMed: 12143050]
- Nightingale KR, Palmeri ML, Bouchard R, Trahey GE. Acoustic radiation force impulse imaging: a parametric analysis of factors affecting image quality. *Proc. 2003 IEEE Ultrasonics Symposium (IEEE)*. 2003
- Nightingale K, Soo MS, Nightingale R, Trahey G. Acoustic radiation force impulse imaging: *in vivo* demonstration of clinical feasibility. *Ultrasound Med. Biol* 2002;28:227–35. [PubMed: 11937286]
- Nightingale KR, Zhai L, Dahl JJ, Frinkley KD, Palmeri ML. Shear wave velocity estimation using acoustic radiation force impulsive excitation in liver *in vivo*. *Proc. 2006 IEEE Ultrasonics Symposium (IEEE)*. 2006
- O'donnell M, Skovoroda A, Shapo B, Emelianov SY. Internal displacement and strain imaging using ultrasonic speckle tracking. *IEEE Trans. Ultrason. Ferroelectr. Freq. Control* 1994;41:314–25.
- Okuda K. Hepatocellular carcinoma. *J. Hepatol* 2000;32:225–37. [PubMed: 10728807]
- Palmeri ML, Nightingale KR. On the thermal effects associated with radiation force imaging of soft tissue. *IEEE Trans. Ultrason. Ferroelectr. Freq. Control* 2004;51:551–65. [PubMed: 15217233]
- Paulsen SD, Nghiem HV, Negussie E, Higgins EJ, Caoili EM, Francis IR. Evaluation of imaging-guided core biopsy of pancreatic masses. *AJR Am. J. Roentgenol* 2006;187:769–72. [PubMed: 16928943]
- Rose SC, Hassanein TI, Easter DW, Gamagami RA, Bouvet M, Pretorius DH, Nelson TR, Kinney TB, James GM. Value of three-dimensional US for optimizing guidance for ablating focal liver tumors. *J. Vasc. Interv. Radiol* 2001;12:507–15. [PubMed: 11287540]
- Rouviere O, Yin M, Dresner MA, Rossman PJ, Burgart LJ, Fidler JL, Ehman RL. MR elastography of the liver: preliminary results. *Radiology* 2006;240:440–8. [PubMed: 16864671]

- Sanada M, Ebara M, Fukuda H, Yoshikawa M, Sugiura N, Saisho H, Yamakoshi Y, Ohmura K, Kobayashi A, Kondoh F. Clinical evaluation of sonoelasticity measurement in liver using ultrasonic imaging of internal forced low-frequency vibration. *Ultrasound Med. Biol* 2000;26:1455–60. [PubMed: 11179620]
- Sandrin L, et al. Transient elastography: a new noninvasive method for assessment of hepatic fibrosis. *Ultrasound Med. Biol* 2003;29:1705–13. [PubMed: 14698338]
- Sharma AC, Soo MS, Trahey GE, Nightingale KR. Acoustic radiation force impulse imaging of *in vivo* breast masses. *Proc. 2004 IEEE Ultrasonics Symposium (IEEE)*. 2004
- Sheafor DH, Paulson EK, Kliewer MA, Delong DM, Nelson RC. Comparison of sonographic and CT guidance techniques: does CT fluoroscopy decrease procedure time? *AJR Am. J. Roentgenol* 2000;174:939–42. [PubMed: 10749226]
- Sheafor DH, Paulson EK, Simmons CM, Delong DM, Nelson RC. Abdominal percutaneous interventional procedures: comparison of CT and US guidance. *Radiology* 1998;207:705–10. [PubMed: 9609893]
- Silverman SG, Sun MR, Tuncali K, Morrison PR, Vansonnenberg E, Shankar S, Zou KH, Warfield SK. Three-dimensional assessment of MRI-guided percutaneous cryotherapy of liver metastases. *AJR Am. J. Roentgenol* 2004;183:707–12. [PubMed: 15333359]
- Sinkus R, Tanter M, Xydeas T, Catheline S, Bercoff J, Fink M. Viscoelastic shear properties of *in vivo* breast lesions measured by MR elastography. *J. Magn. Reson. Imaging* 2005;23:159–65.
- Solbiati L, Goldberg SN, Ierace T, Dellanoce M, Livraghi T, Gazelle GS. Radio-frequency ablation of hepatic metastases: postprocedural assessment with a US microbubble contrast agent—early experience. *Radiology* 1999;211:643–9. [PubMed: 10352586]
- Sommerfeld HJ, et al. Prostate cancer diagnosis using ultrasound elastography. Introduction of a novel technique and first clinical results. *Urologe A* 2003;42:941–5. [PubMed: 12898038]
- Souchon R, Rouviere O, Gelet A, Detti V, Srinivasan S, Ophir J, Chapelon JY. Visualisation of HIFU lesions using elastography of the human prostate *in vivo*: preliminary results. *Ultrasound Med. Biol* 2003;29:1007–15. [PubMed: 12878247]
- Tang S, Li JH, Lui SL, Chan TM, Cheng IK, Lai KN. Free-hand, ultrasound-guided percutaneous renal biopsy: experience from a single operator. *Eur. J. Radiol* 2002;41:65–9. [PubMed: 11750155]
- Torr G. The acoustic radiation force. *Am. J. Phys* 1984;52:402–8.
- Trahey GE, Allison J, Vonramm O. Angle independent ultrasonic detection of blood flow. *IEEE Trans. Biomed. Eng* 1987;34:965–7. [PubMed: 2961682]
- Veit P, Antoch G, Stergar H, Bockisch A, Forsting M, Kuehl H. Detection of residual tumor after radiofrequency ablation of liver metastasis with dual-modality PET/CT: initial results. *Eur. Radiol* 2006;16:80–7. [PubMed: 15868122]
- Weitzel WF, Kim K, Rubin JM, Wiggins RC, Xie H, Chen X, Emelianov SY, O'donnell M. Feasibility of applying ultrasound strain imaging to detect renal transplant chronic allograft nephropathy. *Kidney Int* 2004;65:733–6. [PubMed: 14717949]
- Won HJ, Han JK, Do KH, Lee KH, Kim KW, Kim SH, Yoon CJ, Kim YJ, Park CM, Choi BI. Value of four-dimensional ultrasonography in ultrasonographically guided biopsy of hepatic masses. *J. Ultrasound Med* 2003;22:215–20. [PubMed: 12562126]
- Wood BJ, Khan MA, MCGovern F, Harisinghani M, Hahn PF, Mueller PR. Imaging guided biopsy of renal masses: indications, accuracy and impact on clinical management. *J. Urol* 1999;161:1470–4. [PubMed: 10210375]
- Yeh WC, Li PC, Jeng YM, Hsu HC, Kuo PL, Li ML, Yang PM, Lee PH. Elastic modulus measurements of human liver and correlation with pathology. *Ultrasound Med. Biol* 2002;28:467–74. [PubMed: 12049960]
- Yuen MF, Lai CL. Screening for hepatocellular carcinoma: survival benefit and cost-effectiveness. *Ann. Oncol* 2003;14:1463–7. [PubMed: 14504044]
- Ziol M, et al. Noninvasive assessment of liver fibrosis by measurement of stiffness in patients with chronic hepatitis C. *Hepatology* 2005;41:48–54. [PubMed: 15690481]

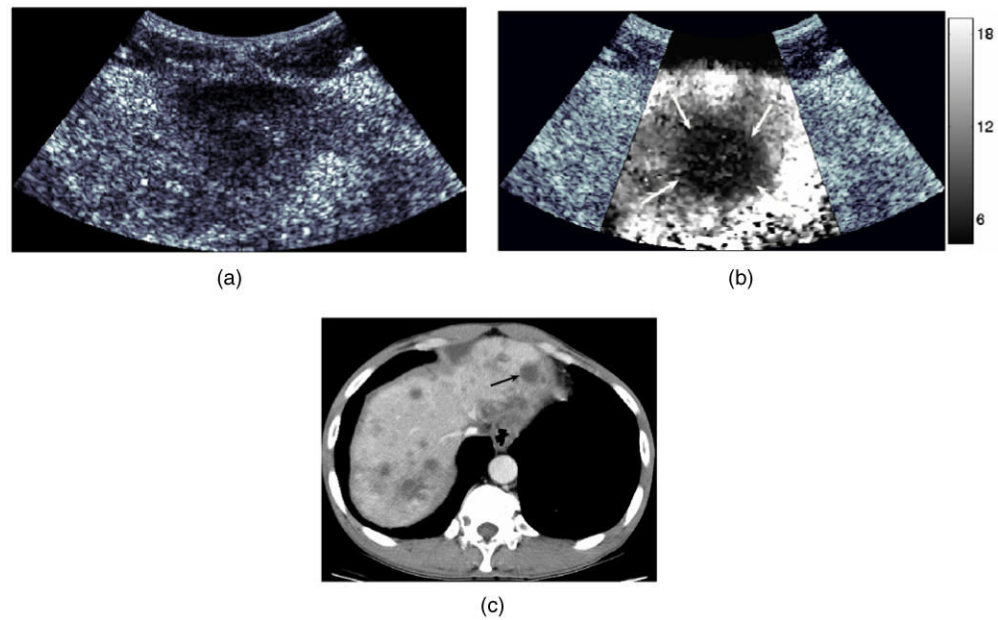


Figure 1.

Transverse B-mode (a), transverse ARFI (b) and axial CT images of a metastasis in the left hepatic lobe of a 62-year-old male. B-mode and ARFI images were acquired with the transducer positioned below the sternum and angled slightly cephalad. ECG-gated acquisition was utilized with data collection occurring 350 ms following the detection of the QRS complex. CT image was acquired during the portal venous phase (PVP) of contrast enhancement. In (a), boundary definition is ambiguous, in part due to the presence of a second, more superficial hypoechoic structure. Definition of the anterior boundary is improved in (b). Solid arrows in (b) indicate boundaries of the mass in the ARFI image. Arrow in (c) indicates lesion in CT image. Scale of ARFI image is displacement in μm .

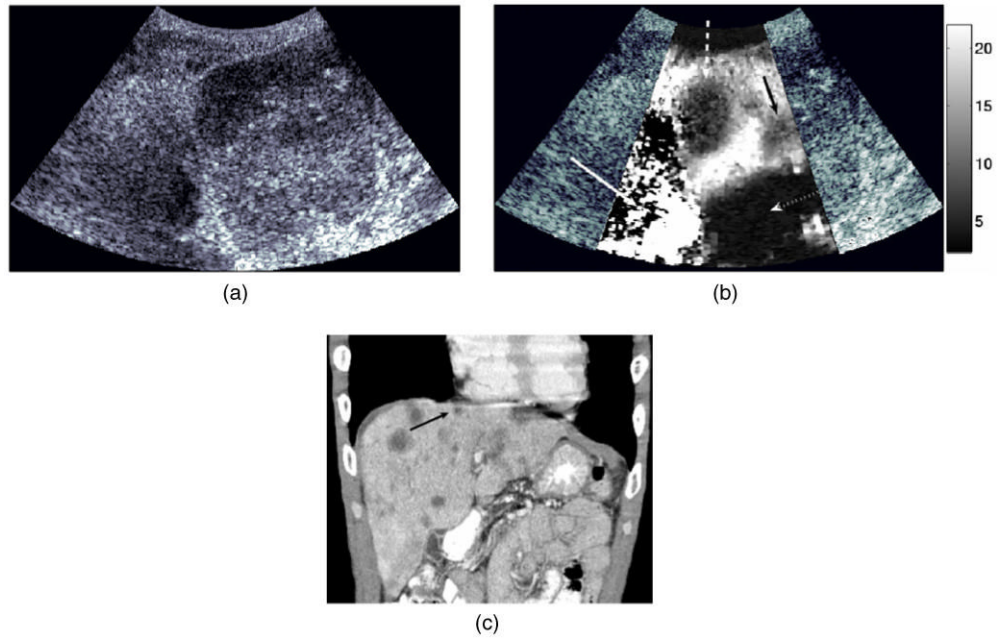


Figure 2. Longitudinal B-mode (a), longitudinal ARFI (b) and coronal CT (c) images of the liver of a 62-year-old male. B-mode and ARFI images were acquired with the transducer positioned slightly right lateral of the mid-sagittal plane. ECG gating was utilized with data collection occurring 350 ms following the detection of the QRS complex. The image plane in (c) is nearly orthogonal to that shown in (a) and (b). Solid white arrow in (b) indicates the heart, broken arrow indicates target tumor, black arrow indicates a portion of a second liver mass and horizontal dashed white arrow indicates a region of low displacement. Arrow in (c) indicates the tumor annotated by broken arrow in (b). Scale of ARFI image is displacement in μm . Note that boundary definition of the target metastasis is improved in the ARFI image relative to the B-mode image, particularly on the medial edge of the lesion. Tissue regions associated with the heart appear as noisy regions with large displacement variance in (b), a result consistent with tissue tracking errors associated with large magnitude and/or high velocity tissue motion (Fahey *et al* 2007). The region of reduced displacement in (b) (indicated by a horizontal dashed arrow) likely originates from the relative magnitude of stationary clutter echoes in this region.

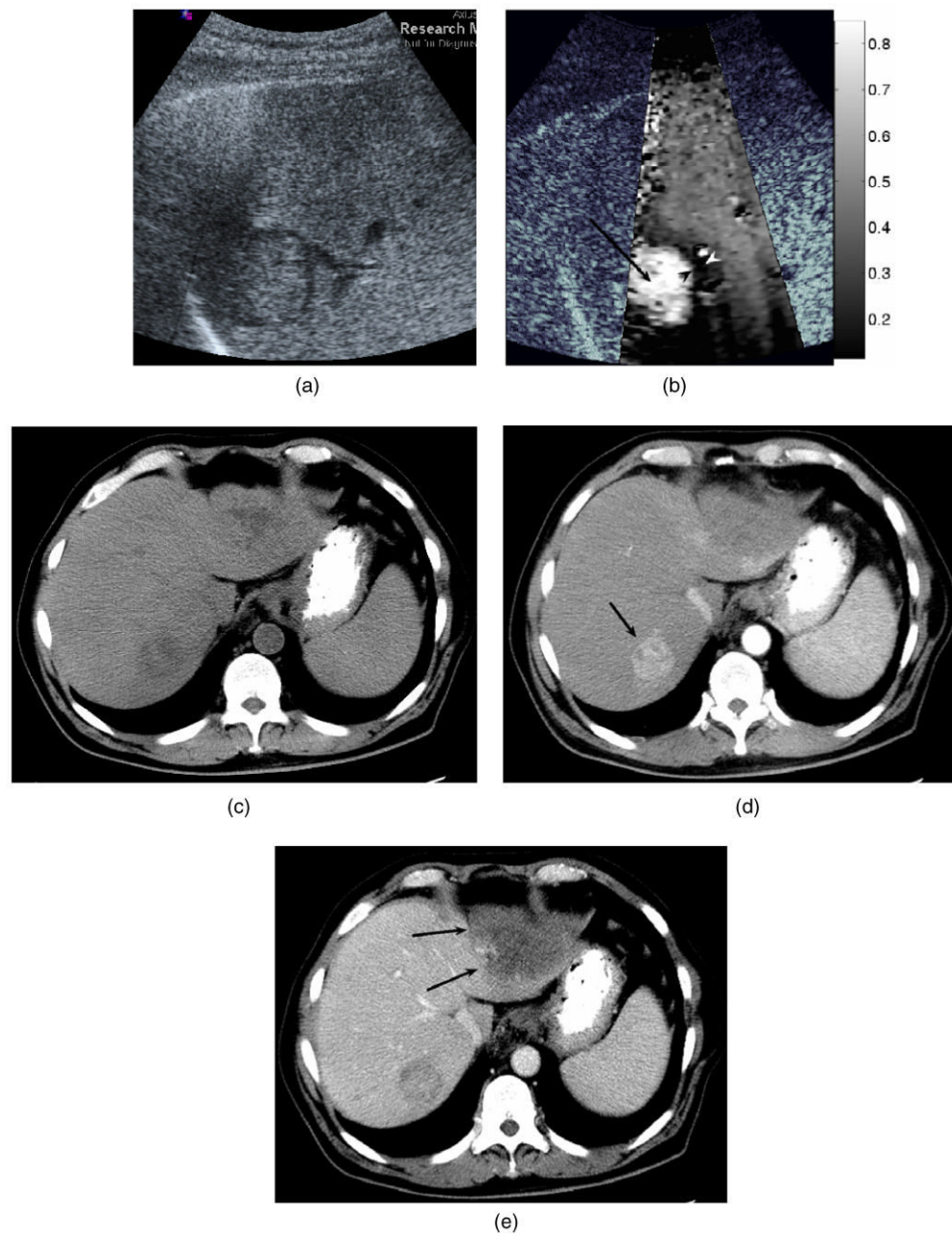


Figure 3.

Screen capture B-mode (a), ARFI (b), unenhanced axial CT (c), axial CT during the hepatic arterial phase (HAP) of enhancement (d) and axial CT during the PVP of enhancement (e) images of a 66-year-old male patient. B-mode and ARFI images were acquired with an intercostal acoustic window along the right anterior axillary line without the use of ECG triggering. Shadowing from the ribs limits image quality near the left side of the B-mode image. Noisy regions of the ARFI image resulting from rib shadowing have been removed. Due to a large range of induced displacements, ARFI data have been log compressed and the image is shown on a logarithmic scale. Arrows in (b) and (d) indicate target tumor. Arrowheads in (b) outline stiff rim surrounding softer tumor, consistent with a fibrous capsule. Patient also had a large hemangioma in the left hepatic lobe, indicated by the arrows in (e).

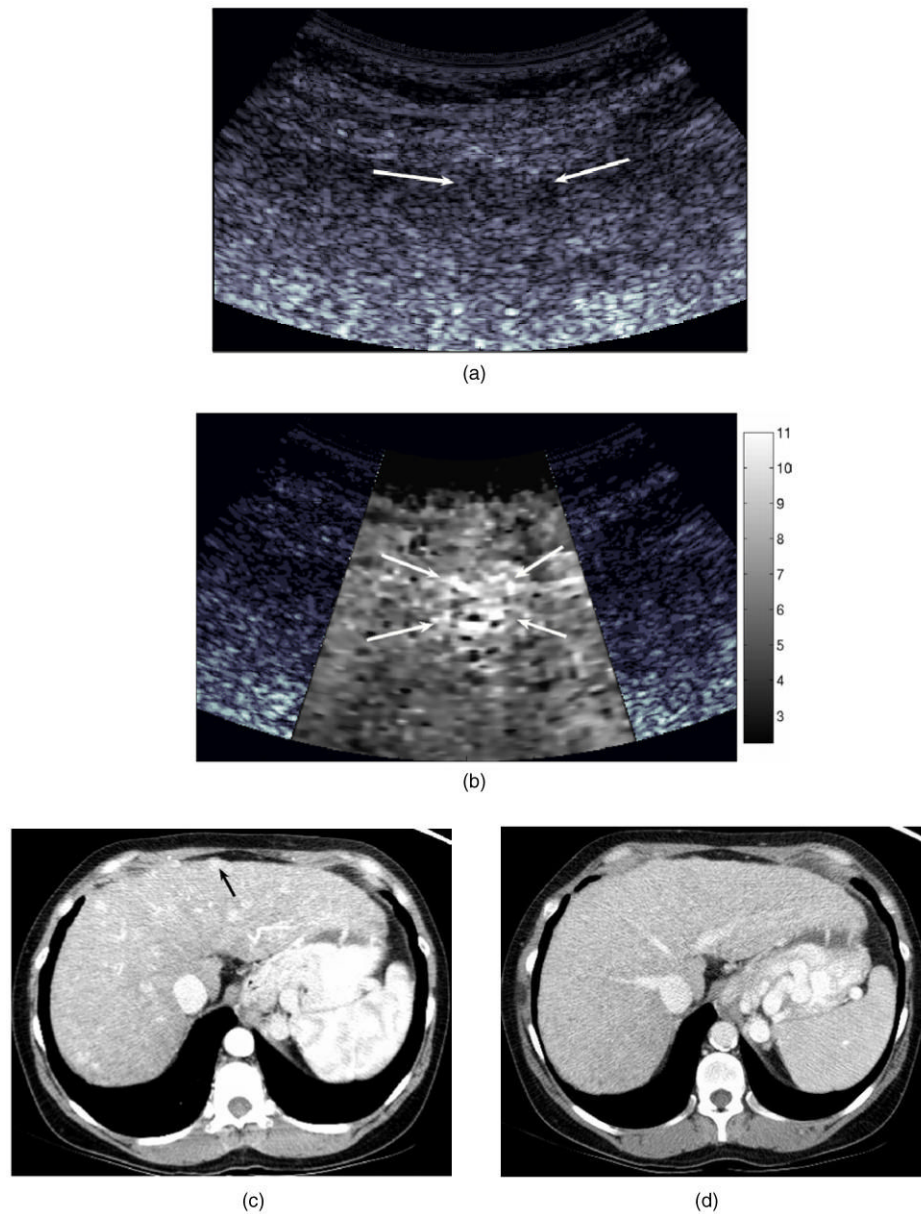


Figure 4.

Images of a suspicious mass in the left hepatic lobe of a 47-year-old female. Shown are transverse B-mode (a), transverse ARFI (b) and contrast-enhanced axial CT images acquired during the HAP (c) and PVP (d). B-mode and ARFI images were acquired with the transducer positioned below the sternum and angled slightly cephalad. ECG-gated acquisition was utilized with data collection occurring 350 ms following the detection of the QRS complex. Arrows in (a) and (b) indicate the apparent boundaries of the mass in the experimental images. Arrow in (c) indicates the mass being biopsied. Scale of the ARFI image is displacement in μm . Although the mass appears with poor boundary definition in (a), boundary definition during live B-mode imaging was marginally better. Boundary definition is relatively better in (b), but remains ambiguous in some regions. Biopsy results did not confirm the presence of malignant tissue, potentially due to the small size of the lesion and its difficult location. However, this patient is being followed with serial imaging to assess the growth of a mass that is highly suspicious for a primary liver tumor (such as HCC) given the setting of cirrhosis.

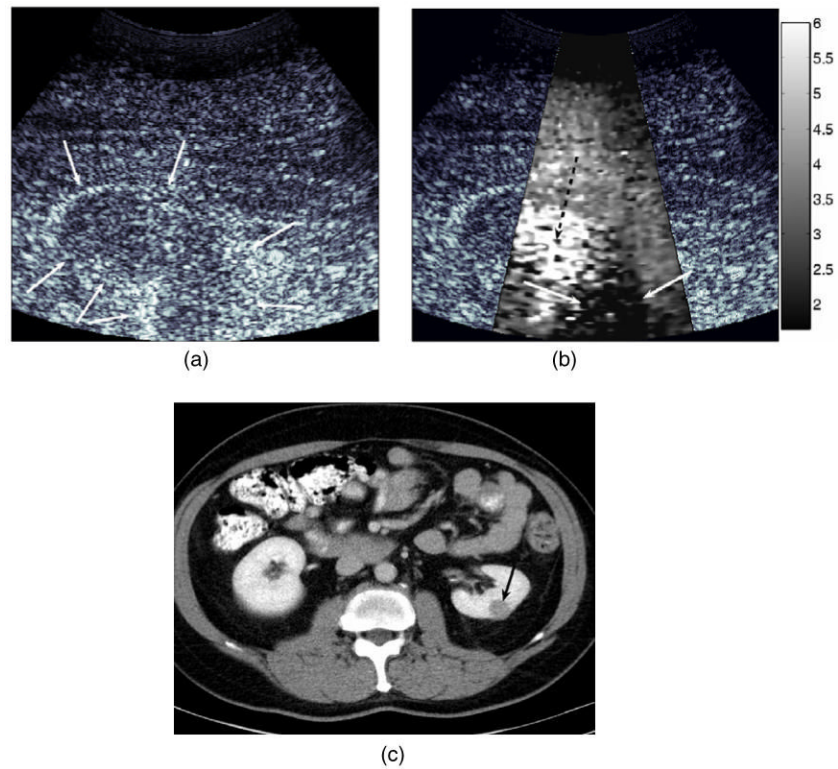


Figure 5. Transverse B-mode (a), transverse ARFI (b) and axial CT (c) images of a small mass in the interpolar region of the left kidney of a 54-year-old male patient. B-mode and ARFI images were acquired with the transducer positioned sub-costally and angled slightly cephalad, without the use of ECG triggering. The ARFI image (b) shows nearly uniform displacement magnitude outside of the kidney, with larger displacements ($\sim 6 \mu\text{m}$, indicated by broken arrow) induced within the non-tumorous renal parenchyma. The malignancy is visualized as a dark region of low displacement at the edge of the kidney (indicated by solid arrows). Arrows in (a) outline boundaries of the kidney. Arrow in (c) indicates the target mass. Scale of the ARFI image is displacement in μm .

Table 1

Contrast of abdominal malignancies in linear B-mode, log-compressed B-mode and linear ARFI images.

	Linear B-mode	Log-compressed B-mode	Linear ARFI
Figure 1	8.9	4.6	13.9
Figure 2	5.5	2.6	9.7
Figure 3	7.1	4.2	11.9
Figure 4	2.8	1.5	3.1
Figure 5	1.5	0.9	10.4
NS 1	8.6	5.2	12.4
NS 2	5.8	2.9	9.2
NS 3	3.7	1.7	5.8
NS 4	5.1	3.2	8.2
NS 5	2.0	1.2	5.7
NS 6	3.6	2.9	9.2

Data values are listed in dB.

NS = not shown, images of these masses are not provided.